https://dx.doi.org/10.1016/j.scs.2022.103718

Investigation of airborne particle exposure in an office with mixing and displacement ventilation

Sumei Liu[a], Mike Koupriyanov[b], Dale Paskaruk[b], Graham Fediuk[b], Qingyan Chen[cd*]
[a]Tianjin Key Laboratory of Indoor Air Environmental Quality Control, School of Environmental Science and Engineering, Tianjin University, Tianjin 300072, China
[b]Price Industries Limited, 638 Raleigh Street Winnipeg, Manitoba R2K 3Z9, Canada
[c]Department of Building Environment and Energy Engineering, The Hong Kong Polytechnic University, Kowloon, Hong Kong
[d]School of Mechanical Engineering, Purdue University, West Lafayette, IN 47905, USA

** Corresponding author's email address: qingyan.chen@polyu.edu.hk (Qingyan Chen)*
E-mail addresses: smliu@tju.edu.cn (Sumei Liu), MikeK@PredictCFD.com (Mike Koupriyanov), DaleP@priceindustries.com (Dale Paskaruk), GrahamF@priceindustries.com (Graham Fediuk)

HIGHLIGHTS

- Measurements of particle number distribution under mixing ventilation, displacement ventilation system in an office
- Comparison of the effects of different air change rates on indoor air quality
- Verification of the computed results with corresponding experimental data

ABSTRACT

Effective ventilation could reduce COVID-19 infection in buildings. By using a computational fluid dynamics technique and advanced experimental measurement methods, this investigation studied the air velocity, air temperature, and particle number concentration in an office under a mixing ventilation (MV) system and a displacement ventilation (DV) system with different ventilation rates. The results show reasonably good agreement between the computed results and measured data. The air temperature and particle number concentration under the MV system were uniform, while the DV system generated a vertical stratification of the air temperature and particle number concentration. Because of the vertical stratification of the particle number concentration, the DV system provided better indoor air quality than the MV system. An increase in ventilation rate can reduce the particle concentration under the two systems. However, the improvement was not proportional to the ventilation rate. The increase in ventilation rate from 2 ACH to 4 ACH and 6 ACH for MV system reduced the particle concentration by 20% and 60%, respectively. While for the DV system, increasing the ventilation rate from 2 ACH to 4 ACH and 6 ACH reduced the particle concentration by only 10% and 40%, respectively. The ventilation effectiveness of the MV system was close to 1.0, but it was much higher for the DV system. Therefore, the DV system was better than the MV system.

Keywords: Indoor air quality, experimental measurements, RNG k-ε model, CFD, ventilation effectiveness

1. Introduction

The novel coronavirus disease (Covid-19), caused by the SARS-CoV-2 virus, has spread throughout a wide geographic area [1, 2], creating significant social and economic disruptions in various countries [1], and causing more than 5.5 million deaths as of the mid-January 2022 [2]. The vast majority of COVID-19 infections occurred in and around buildings. It is important to explore how to improve air quality in buildings and cities for creating sustainable and socially resilient cities. Multiple studies have demonstrated that the virus may remain viable after aerosolization in the indoor environment [3,4,5]. Small droplets ($d \leq 100$ μm) can remain airborne for significant lengths of time (from tens of seconds to several minutes) and can thus be inhaled, depending on the indoor airflow patterns [6]. Therefore, it is important to explore the effect of indoor airflow pattern on indoor disease spread and control.

Ventilation is a primary infectious disease control strategy that dilutes the air in a room and removes virus aerosols [7,8]. The mixing ventilation (MV) system has been the most popular and widely used air conditioning system for decades [9,10]. However, with the MV system, all the air in an indoor space room is mixed and diluted with supplied air to maintain the air quality in that space. Therefore, the contaminated air spreads throughout the room, even to areas that were not originally contaminated. In contrast, the displacement ventilation (DV) system is designed to minimize the mixing of air in indoor space by maintaining a one-dimensional plug flow. In the DV system, cool air is supplied to the lower level of the room with low momentum [11]. The supplied air spreads throughout the lower level of the room due to thermal buoyancy until it encounters heat sources. It then rises upward with the thermal plume generated by the heat sources. Typically, a contaminant source is associated with heat sources. The thermal plumes can therefore draw the contaminated air to the upper part of the room, where it will be exhausted at ceiling level. The DV system is a promising approach for enhancing ventilation performance and reducing the risk of airborne infection indoors [12,13]. The system can also be energy efficient [14,15].

Many studies have been conducted to compare the performance of MV and DV systems by using experimental measurements and/or CFD simulation. For example, Hirnikel [16] used CFD to calculate the particle transmission in a test room with MV and DV systems. They found that the DV system could effectively contain the heated contaminants stratified near the ceiling. This implied the air in the breathing zone was cleaner. Li et al. [17] also found that the inhaled dose was the lowest under DV for smaller droplets. However, experimental measurements from Yin et al. [18] found that DV may or may not provide a better air quality in a ward, depending on the location of the exhaust in relation to the restroom. Gao et al. [19] showed that exhaled droplets during normal breathing could be trapped in the breathing zone by thermal stratification under DV, which might lead to a higher exposure risk for other co-occupants. In addition, the exposure to the contaminants was sensitive to the source locations under DV, but little under MV [20,21]. These investigations mainly compared the performance of MV and DV. However, few investigations further compared the influence of ventilation rates for the two ventilation systems.

In addition to airflow pattern, ventilation rate has been recognized as a key factor in airborne disease transmission [22]. Previous studies have reported an association between insufficient ventilation and increased risk of infection by diseases such as measles, tuberculosis, chickenpox, influenza, smallpox, and SARS [8, 23]. Kulkarni et al. [24] and Sornboot et al. [25] found that with low ventilation rates in indoor environments, the infection probability would rise among the occupants in enclosed spaces. ASHRAE [26], the Federation of European Heating, Ventilation and Air-Conditioning Associations (REHVA) [27], the CDC [28], and the WHO [29] recommend measures related to the increase in ventilation rates and filtration efficiencies for public buildings in the context of COVID-19. Although higher air change rates

can better dilute contaminate concentrations in a room, increasing the air change rate alone may not effectively reduce airborne infection [30,31]. Mousavi and Grosskopf [32] found that higher ventilation rates were not proportionately effective in reducing aerosol concentrations, because airflow pattern plays an important role. Therefore, it is important to compare the effects of different ventilation modes and ventilation rates on indoor air quality.

To evaluate the transmission of airborne particles in an indoor space, most studies have employed experimental and numerical methods. Careful design of experiments can replicate reality in a controlled environment and provide reliable information [33]. However, experimental measurements are time-consuming and costly. In addition, the size of an experimental chamber is often fixed, and the simulated scenario is generally limited [34]. With the development of computer methods, researchers have increasingly adopted computational fluid dynamics (CFD) for the calculation of indoor airflow [35] and airborne particle transmission [36]. CFD simulation can provide very detailed information about airflow and particle distribution at a much lower cost than that of the experimental approach. However, CFD uses numerical models to approximate turbulence and thermo-fluid boundary conditions, which can lead to errors [37]. Therefore, it is vital to use measured data to validate CFD results.

This investigation measured the air velocity, temperature, and particle concentration in an office with an MV system and a DV system. A CFD model was also utilized to simulate the airflow pattern and particle transmission for the two ventilation systems. The effects of different ventilation modes and ventilation rates on indoor air quality were comprehensively compared. The results were used to assess the performance of the two ventilation systems.

Section 2 described research method of experimental measurement and CFD simulation for an office with MV and DV system. In addition, indices for evaluating indoor air quality were presented. In Section 3, the results of different airflow pattern and ventilation rates on indoor air quality were given. Section 4 discussed the limitations of this investigation before conclusions were presented in Section 5.

2. Research Method

2.1 Experimental chamber for simulating an office with a mixing ventilation system and a displacement ventilation system

To compare the performance of mixing and displacement ventilation systems, this investigation used an environmental chamber to simulate a typical open office, as depicted in Fig. 1. The chamber was 7.0 m long, 5.8 m wide, and 3.05 m high, with four heated manikins, four computers, and four tables. The manikins were heated by a 120 V direct electrical current, and the sensible heat production for each manikin was controlled at around 80 W. On the ceiling of the chamber, there were ten lighting panels with 640 W power input. The test chamber was equipped with MV and DV systems, as shown in Fig. 1. In the MV system, fresh air was supplied through two diffusers installed in the ceiling and exhausted through a ducted return in the corner of the ceiling. In the DV system, fresh air was supplied through one diffuser located at floor level in the center of one of the side walls. The return location was the same as that for the MV system.

The office chamber was ventilated by a closed-loop air-conditioning system with all of the supply air passing through an EN-1822 class H-14 HEPA filter. Particle measurements were taken in the supply ducts prior to testing, to ensure that the supply air was free of particles. With the use of a rotating vane anemometer, RTD temperature sensors, and LabView control software, the supply-air flow rate and temperature could be adjusted to achieve the necessary experimental conditions. The error for airflow measurement was ±5%. The test chamber was carefully sealed before the experiments, and the exhaust ran at 0.85 times the supply airflow to

ensure a positive pressure of 0.025 Pa. It was to eliminate infiltration into the test chamber and keep the background particle concentrations low.

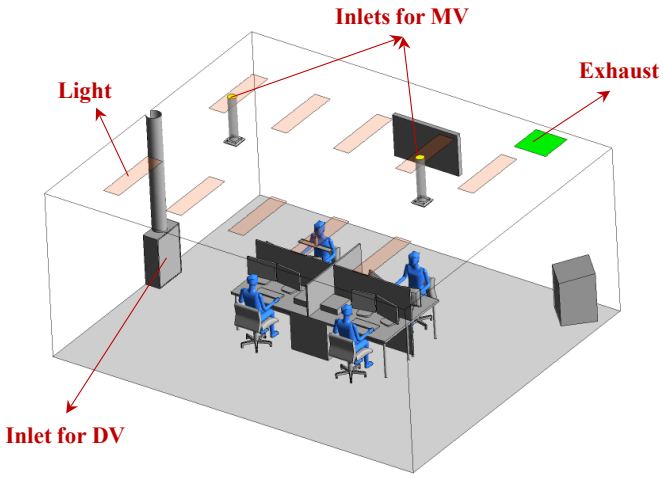

Fig. 1. The layout of the chamber

2.2 Experimental setup

Air velocity, air temperature, and contaminant concentration provide vital information about indoor air quality and thermal comfort and were therefore measured in this study. Before each measurement, the HVAC system was run until the room reached steady-state thermal conditions. The air temperature and velocity were then recorded, and the particle experiment proceeded. Omni-directional hot-sphere velocity transducers and PT100 RTD temperature sensors were used to measure the air velocity and air temperature, respectively, inside the chamber. The air velocity measurement error was ±0.02 m/s, and the error for temperature measurement was ±0.2 °C.

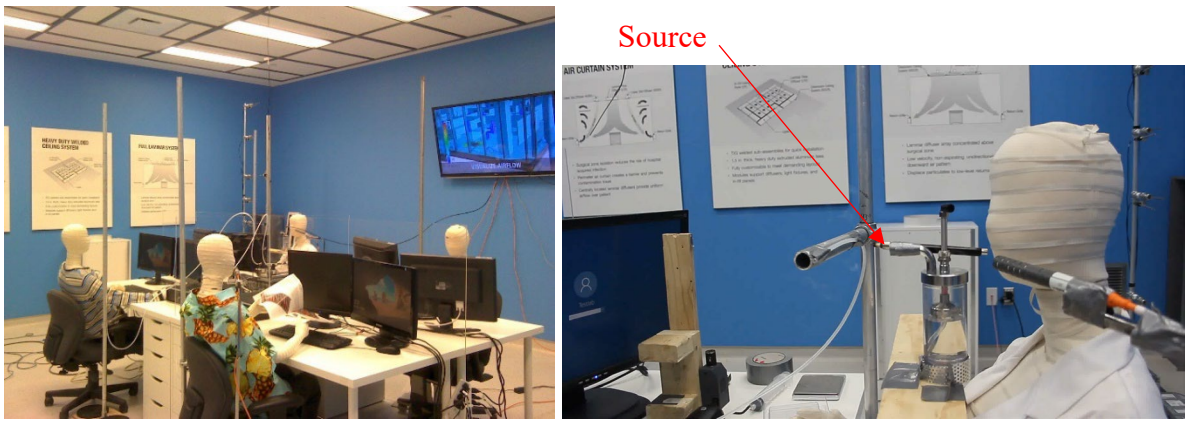

Fig. 2. Photograph of environmental chamber

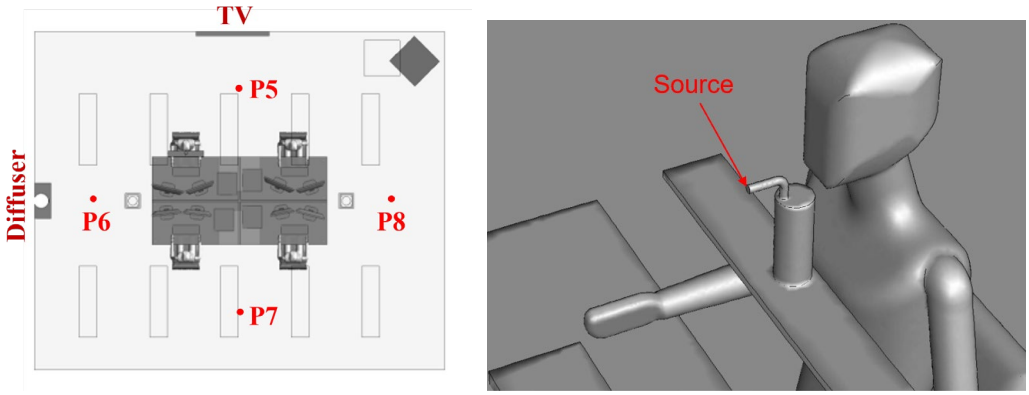

(a) (b)

Fig. 3. (a) Measurement locations, (b) Particle source in CFD model

Growing evidence [38,39] has suggested that the SARS CoV-2 could be transmitted through air [40,41], and the virus in the small aerosol particles can survive in the air for hours. Therefore, this study aims at studying the airborne particle transmission. Gupta et al. [42] found that the evaporation of droplets with an initial diameter less than 30 µm can be ignored since they would drop to floor quickly. Morawska [43] found that droplets with a diameter up to 10 µm can evaporate within one second and were reduced to droplet nuclei or residue core. Our study used the droplet nucleus directly for the evaluation of particle transmission and neglected the evaporation of the particles either in the experimental measurements or CFD simulations.

A low-flow 4-jet BLAM (Blaustein Atomizer) with 0.9% saline solution (NaCl – similar to the solution in human saliva) was utilized to introduce particles into the space. The saline droplet evaporated quickly to form a solid droplet residue. As shown in Fig. 2b, the particle source was located 0.02 m in front of the mouth of thermal mannequin A. Particles were introduced into the room with the use of constant compressed air at 1.034 bar, cycling 0.8 seconds on and 1.2 seconds off. The source generated a range of particle sizes, from 0.3 µm to 2 µm, and allowed for an average particle concentration that was more than 10x that of the background readings. The flow rate of the BLAM was 0.003 mL/min. The jet velocity of the BLAM was 1.58 m/s and the source temperature was within 0.1°C of the room temperature. It was used to simulate the manikin breathing out. Previous investigation [44] reported that viral respiratory infected individuals shed virus into the environment by coughing, sneezing, talking, and breathing. This investigation focused on particles with a diameter of 0.4 µm, which was used to represent breathing in previous investigations [36,42]. Future studies can expand the diameter to cover particles in all sizes generated by a patient.

Two Fluke 983 handheld particle counters in combination with a constructed sampling tree were used to measure the particle concentrations throughout the space. The particle concentration error was ±15% of the reading. The sampling tree was constructed from solenoids and polyethylene-lined tubing with an ethyl vinyl acetate shell for sampling at different points. The tubing was tested at different lengths to ensure minimal particle loss while sampling. The sampling tree maximized the number of sample points during a single test without disruption of the test space.

The weight of the BLAM was measured before and after the test to determine the volume of particles introduced into the room. Particle counters were zeroed with the use of the manufacturer's zero filters. Once a thermal balance was achieved, particles were monitored until background levels were $< 0.05/cm^3$ and showed no signs of deviation for three consecutive readings of 15 minutes. When the background concentration had stabilized and had been logged for 30 minutes, particles were introduced. The particle concentration was monitored until a stable concentration was achieved, with no increasing or decreasing trend

over three consecutive 15-minute intervals. The particle concentration was then logged for 30 minutes. The solenoids were switched to the next measurement point, a steady state was again reached as described above, and the particle concentration was logged for 30 minutes. This procedure was repeated until all points had been logged.

So that the experiment was not disturbed, some boundary conditions were measured separately. A thermal camera was used to measure temperatures on walls and heated surfaces. Because space is limited, only the average surface temperature of the 4 ACH (air changes per hour) MV system is presented here. Table 1 summarizes the thermo-flow boundary conditions for 4 ACH MV system. The total air supply rate for the 4 ACH MV system was 443.9 m^3/h.

Table 1. Overview of basic thermo-flow boundary conditions for 4 ACH MV system

Boundary surface	Boundary Type	Value
Left-hand diffuser inlet	Velocity-inlet	12.9°C, 3.5 m/s (Normal to the boundary) Turbulent intensity: 15% Turbulent length scale: 0.01 m
Right-hand diffuser inlet	Velocity-inlet	12.5°C, 3.5 m/s (Normal to the boundary) Turbulent intensity: 15% Turbulent length scale: 0.01 m
Thermal manikin	Non-slip Wall	31°C
Left-hand TV display	Non-slip Wall	30.2°C
Computer	Non-slip Wall	33°C
Computer monitor	Non-slip Wall	29.6°C
Floor	Non-slip Wall	24°C
Left-hand wall	Non-slip Wall	25°C
Right-hand wall	Non-slip Wall	25.2°C
Front wall	Non-slip Wall	25°C
Back wall	Non-slip Wall	25.6°C
Return	Pressure-outlet	22.1°C, Pa = 0

To explore the influence of different air flow rates on indoor air quality, three ACHs were measured for each ventilation system. ISO 17772-1:2017 [45] and EN 16798-1:2019 [46] recommended 1.5-2 l/s per floor m² (10-15 l/s per person) outdoor airflow rates in offices and about 4 l/s per floor m² (8-10 l/s per person) in meeting rooms and classrooms. There is currently no international standard for a minimum ventilation rate that would sufficiently prevent the risk of COVID-19 disease transmission in indoor spaces. WHO [47] recommended a ventilation rate of at least 10 l/s per person. This investigation explored three different ventilation rate, as summarized in Table 2. Note that different air supply temperatures were used for different air flow rate cases to maintain a similar indoor thermal environment. Table 3 summarizes the air flow rate and air temperature at the supply and exhaust and in the room.

Table 2. Experimental airflow rates and the corresponding thermal loads

		Airflow (l/s per floor area m^2)	Airflow (l/s per person)	Thermal Load (W/m^2)
MV	2 ACH	1.5	15.7	73
	4 ACH	3.0	30.8	113
	6 ACH	4.6	46.3	113
DV	2 ACH	1.5	15.7	73
	4 ACH	3.1	31.6	113
	6 ACH	4.5	46.0	113

Table 3. Air temperature at the supply and exhaust and in the room for the two ventilation systems (Unit: °C)

		Diffuser 1 (Left)	Diffuser 2 (Right)	DV Diffuser	Room	Exhaust
MV	2 ACH	13.4	12.6	N/A	22.0	22.2
	4 ACH	12.9	12.5	N/A	22.7	22.1
	6 ACH	16.1	16.1	N/A	22.1	22.3
DV	2 ACH	N/A	N/A	13.9	22.9	22.4
	4 ACH	N/A	N/A	16.7	23.4	23.6
	6 ACH	N/A	N/A	19.5	23.7	24.1

2.3 CFD modeling of indoor environment

This investigation used a commercial CFD program, ANSYS Fluent 14.0 [48], to simulate the airflow pattern and particle distribution in the office. The simulation used steady-state Reynolds-averaged Navier-Stokes (RANS) equations with the RNG k-ε turbulence model [49] to solve the airflow and temperature fields in the indoor space. The standard wall function was utilized for walls to describe the near-wall velocity distribution. The governing transport equations were solved by means of the finite volume method. The numerical method used the SIMPLE algorithm for coupling the pressure and velocity equations, and the second-order discretization schemes for the convection and viscous terms of the governing equations. The results were considered to have converged when the residuals for all the independent parameters reached 10^{-4}.

CFD solves the governing conservation equations of mass, momentum, energy in the following general form:

$$\rho \frac{\partial \bar{\phi}}{\partial t} + \rho \bar{u_\iota} \frac{\partial \bar{\phi}}{\partial x_i} - \frac{\partial}{\partial x_i}\left[\Gamma_{\phi,eff} \frac{\partial \bar{\phi}}{\partial x_i}\right] = S_\phi \quad (1)$$

where ρ is air density (kg/m^3), ϕ stands for u_i, E in momentum equation and energy equation, respectively, t time (s), u_i the Reynolds time-averaged velocity component in the x_i (*i, j =1, 2, 3*) directions, respectively, $\Gamma_{\phi,eff}$ the effective diffusion coefficient, and S_ϕ the source term. When ϕ *= 1,* $\Gamma_{\phi,eff}$ and S_ϕ equal zero, Equation (1) becomes the continuity equation. Besides, this simulation assumed air density varied with air temperature by employing the Boussinesq approximation [50], which is valid since the air density variation in the indoor environment was sufficiently small.

Equation (1) can be solved by approximating turbulence quantities with the turbulence model. This study has used the RNG k-ε turbulence model to solve the airflow and temperature fields in the indoor space [49]. In the RNG k-ε model, the transport equations of turbulence kinetic energy k and its dissipation rate ε are:

$$\frac{\partial(\rho k)}{\partial t} + \frac{\partial(\rho k u_i)}{\partial x_i} = \frac{\partial}{\partial x_j}\left[(\nu + \frac{\nu_t}{\sigma_k})\frac{\partial k}{\partial x_j}\right] + G - \mathrm{E} \quad (2)$$

$$\frac{\partial(\rho \mathrm{E})}{\partial t} + \frac{\partial(\rho \mathrm{E} u_i)}{\partial x_j} = \frac{\partial}{\partial x_j}\left[(\nu + \frac{\nu_t}{\sigma_\varepsilon})\frac{\partial \mathrm{E}}{\partial x_j}\right] + C_{\varepsilon 1}\frac{\mathrm{E}}{k}G - C_{\varepsilon 2}\frac{\mathrm{E}^2}{k} - C_\mu \eta^3 \frac{1-\eta/\eta_0}{1+\beta\eta^3}\frac{\varepsilon^2}{k} \quad (3)$$

where ρ is air density (kg/m^3), t time (s), u_i and u_j the Reynolds time-averaged velocity component in the x_i and x_j ($i, j = 1, 2, 3$) directions, respectively, ν the dynamic viscosity of air (m^2/s), $\nu_t = C_\mu \frac{k^2}{\varepsilon}$ the turbulence kinematic viscosity (m^2/s), $\sigma_k = 0.7194$ the turbulence effective Prandtl number for k, G the source term, $\sigma_\varepsilon = 0.7194$ the turbulence effective Prandtl number for ε, $C_{\varepsilon 1} = 1.42$, $C_{\varepsilon 2} = 1.68$, $C_\mu = 0.085$, $\eta = (2E_{ij} \cdot E_{ij})^{1/2} \frac{k}{\varepsilon}$, $E_{ij} = \frac{1}{2}(\frac{\partial u_i}{\partial x_j} + \frac{\partial u_j}{\partial x_i})$, $\beta = 0.012$, and $\eta_0 = 4.38$.

This study used non-slip boundary conditions for velocity on walls and heated surfaces in the computational domain, and the corresponding temperatures were set according to the measurements. For the MV system, the exact geometry of the diffusers was modeled. The calculation domain was extended at the diffuser inlet to obtain fully developed flow and to avoid reversed flow. The inlets of the duct were set as velocity-inlet. The inlet velocity was uniform and set to 3.5 m/s for the 4 ACH scenario. The exhaust was modeled as pressure-outlet. For the DV system, this investigation used a rectangular perforated diffuser to supply conditioned air to the room. Around 20% of the diffuser's inlet surface was perforated, as shown in Fig. 4(a). Perforated diffusers cannot be treated as simple openings in CFD simulations because their effective area ratios are small. Zhang et al. [51] developed a simple method to describe a diffuser, by directly specifying the correct jet momentum from the diffuser while adjusting the airflow rate by changing the effective areas. This investigation used the method of Zhang et al. to describe the inlet velocity boundary condition of the diffuser, which was realized by means of a user-defined function (UDF) in ANSYS Fluent. Fig. 4(b) presents the simulated air velocity distribution on the diffuser face. Fig. 5 compares the simulated velocity with the measured data, at a distance of 0.025 m from the front of the diffuser face. The simulated distribution of the velocity was in good agreement with the corresponding data. The maximum difference between the simulated results and the measured data was 0.2 m/s.

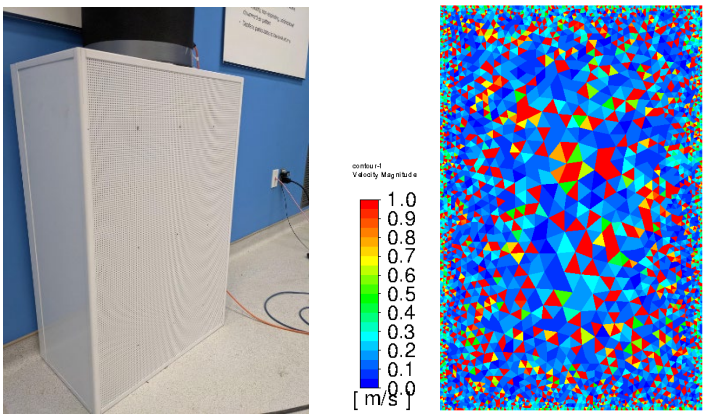

(a) (b)

Fig. 4. (a) Photograph of the diffuser and (b) mesh cells coloured by velocity of the diffuser using random blocking method

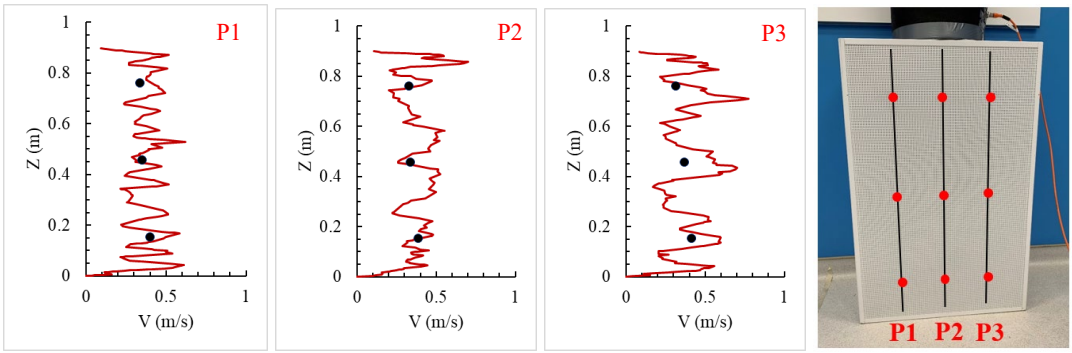

Fig. 5. Comparison of simulated velocity with measured data in front of the diffuser (Line: CFD, Black dot: measured data)

This investigation used the Lagrangian method to track individual particle motion based on the CFD-calculated airflow distribution. The turbulent flow was treated as a continuous phase and simulated in the Eulerian frame. A previous investigation [52] found that the pressure gradient force and the virtual mass force could be neglected due to the small ratio of air density to particle density. Saffman's force and the Brownian force have an effect only on sub-micron particles [53]. Considering the small number of aerosol particles in indoor air, collisions among particles can also be neglected [54,55]. Therefore, this investigation did not consider them in the particle movement equation. The Lagrangian method determines the particle model in accordance with Newton's law:

$$\frac{du_p}{dt} = \frac{18\mu_a}{\rho_p d_p^2 C_c}\left(u_a - u_p\right) + \frac{g(\rho_p - \rho_a)}{\rho_p} \tag{4}$$

where the first and second terms on the right-hand side represent the drag force and gravity term, respectively, μ_a air viscosity, d_p particle diameter, u_p particle velocity, u_a air velocity, g gravitational acceleration, ρ_p particle density, ρ_a air density, and C_c the Cunningham correction factor. The factor can be expressed as:

$$C_c = 1 + \frac{2\lambda}{d_p}(1.257 + 0.4\exp\left(-1.1d_p/2\lambda\right) \tag{5}$$

where λ is the mean free path of air molecules.

Turbulent dispersion, which is associated with instantaneous flow fluctuations, is one of the main mechanisms of particle spreading. This study used the discrete random walk (DRW) model [48] to calculate the turbulent dispersion of particles. One-way coupling was used to simulate the interaction between the airflow and particles, which means that flow has an impact on particle motion but not vice versa.

The particle density was 1004.6 kg/m^3. This investigation released 200 spherical particles at each time step of 0.1 s to obtain a statistical particle distribution according to Chen et al. [56,57]. The total simulation time was 600 s. Therefore, the total number of particles emitted to the domain was 1.2 million. The exact geometry of the particle emitter was constructed in the CFD model, as shown in Fig.3(b). The particles were injected at the outlet of the emitter, which was the same as the experiment. The jet velocity and temperature at the source were set according to the experimental data. Table 1 summarizes the boundary conditions used for the 4 ACH mixing ventilation system.

A previous study found that particle deposition on walls may be overestimated due to the assumption of isotropic turbulence in near-wall regions [58]. The present investigation

assumed no particle deposition, so particles were reflected once they reached a wall. When a particle passed through the exhaust, the calculation of the particle trajectory ended. The present study used ANSYS Fluent to calculate the airflow and the Lagrangian trajectories. However, the Lagrangian method does not directly calculate the particle concentration. Therefore, this study employed a user-defined function (UDF) [59] to calculate the concentration distribution from the trajectories. The particle source in-cell (PSI-C) scheme was used to correlate the concentration with the trajectories on a computational cell basis [59]:

$$\overline{C_J} = \frac{\dot{M} \sum_{i=1}^{n} dt_{(i,j)}}{V_j} \tag{6}$$

where $\dot{M}$ is the number flow rate of each trajectory, V is the volume of a computational cell for use in concentration calculations, *dt* is the particle residence time, and subscript (i,j) represents the i^{th} trajectory and the j^{th} cell, respectively.

Gambit software (version 2.4.6) [60] was used to generate a discrete grid for discretizing the governing transport equations. Because of the complexity of the geometric model, this study used the tetrahedral grid scheme, which can be adapted to various geometric structures. We tested grids with 5, 9, and 16 million cells. Our simulations found that the grid number of 9 million provided grid-independent results. Grid independence analysis can be found in Appendix I.

2.4 Indices for evaluating indoor air quality

The normalized contaminant concentration, C^*, was employed to evaluate air quality in the room [61]. It is defined as:

$$C^* = \frac{C - C_s}{C_e - C_s} \tag{7}$$

where C, C_e, and C_s are the contaminant concentration at a particular location, at the exhaust, and at the supply (C_s = 0), respectively. The contaminant concentration can be number concentration or mass concentration. Since the diameter and density of the particle is fixed, the C^* is the same for number and mass concentration.

Since the particle concentration in the breathing zone of the occupants was of great importance, this investigation also calculated the ventilation effectiveness [62,63] of the two ventilation systems as:

$$VE_a = \frac{C_e - C_o}{C - C_0} \tag{8}$$

where C_o, C_e, and C are the contaminant concentration of outdoor air (C_o = 0), at the exhaust, and in the breathing zone. If the room air is perfectly mixed by a ventilation system, VE_a is equal to 1. The larger the VE_a is, the better the air quality should be. Previous investigations [59,64] have used above parameters to evaluate indoor air quality of particle transmission. Therefore, this investigation adopted these parameters to conduct the comparison.

3. Results

This section summarizes the flow characteristics of the mixing ventilation system under 4 ACH, the displacement ventilation system under 4 ACH, and a comparison of the effects of different ventilation rates on indoor air quality for the two ventilation systems.

3.1 Air distribution in the room with the mixing ventilation system under 4 ACH

This section summarizes the flow characteristics of the MV system with 4 ACH. Fig. 6(a) presents the simulated velocity and temperature distributions in the center section of the room. We set a uniform air speed at the duct inlets at the top of the figure. The air moved through the diffusers and then attached to the ceiling due to the Coanda effect. The air traveled downward when it reached the side walls, and the two jets met in the middle of the room. Fig. 6(b) depicts the temperature and velocity distributions in the section through the two occupants. The results show that the temperature in the room was highly uniform. The air moved upward around the occupants due to the thermal plumes that they generated.

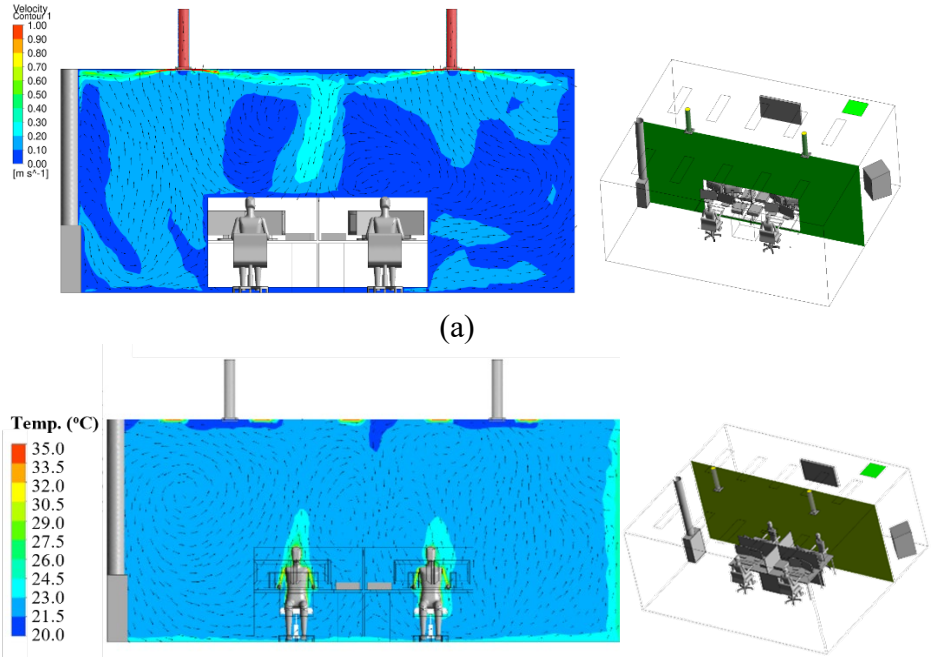

Fig. 6. Simulated air velocity and temperature distributions in the office: (a) in the center section of the room, (b) in the section through the two occupants.

Fig. 7 illustrates the simulated particle distribution in the section through the source person in the room. The particles were drawn upward by the thermal plume generated by the source person. The particles then spread throughout the whole room with the airflow formed by the MV system. Although there was a partition on the table between the occupants, the particles could easily spread from the source into the breathing zone of the other person. This is because, under the MV system, all the air in the room was mixed and diluted with supplied air to maintain the air quality. Note that the high concentration at the left wall was due to the vortex generated near the floor. The particles were easily concentrated in the recirculation zone.

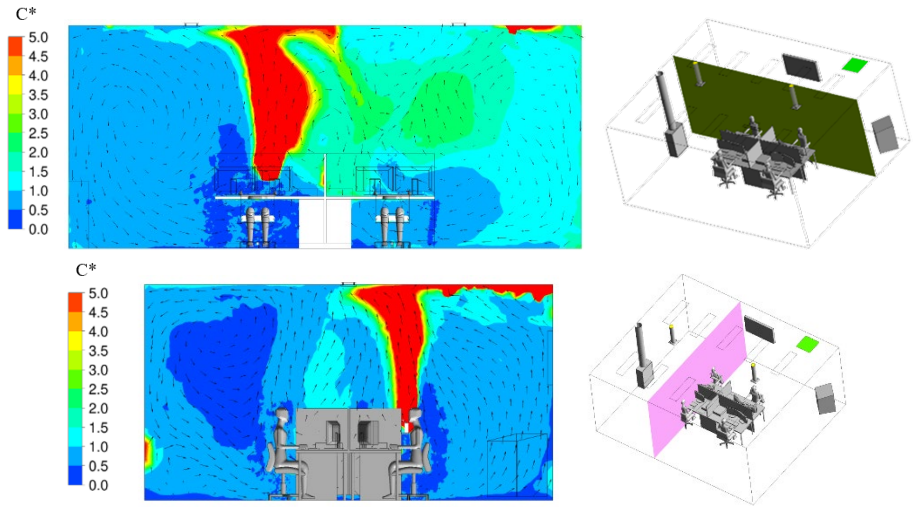

(a) (b)

Fig. 7. Simulated particle concentration in different sections of the room

Fig. 8 compares the measured and computed air temperature, air velocity, and particle concentration in the office with the MV system under 4 ACH. The measured and computed temperature was determined at locations P5, P6, P7, and P8, as shown in Fig. 3. The air temperature was very uniform at 22.4 ºC along the vertical line and at different locations. The air velocity in the room was lower than 0.2 m/s, except near the ceiling in locations P6 and P8 due to their proximity to the diffusers. The normalized particle concentration at different measuring locations was around 1, which indicates perfect mixing. The simulated results agreed reasonably well with the measured data. The maximum differences between the simulated results and measured data for temperature, air velocity, and normalized concentration were 1 ºC, 0.01 m/s, and 1.0, respectively. The simulated velocity at most measuring points was within the error range. For particle concentration, the largest difference was found in position 6, which was located on the left side of the room. The simulated results show that one large vortex formed on the left of the room, as depicted in Fig. 7(a), which may block the particle transmission to position 6.

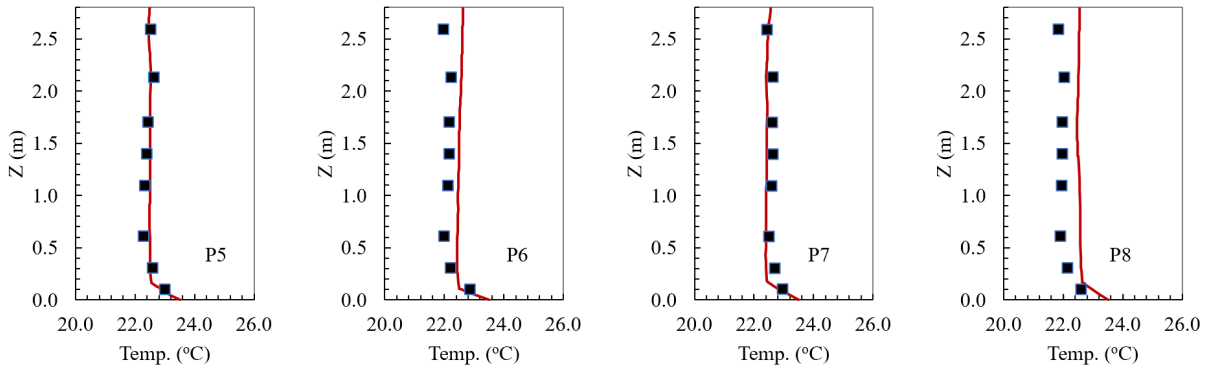

(a)

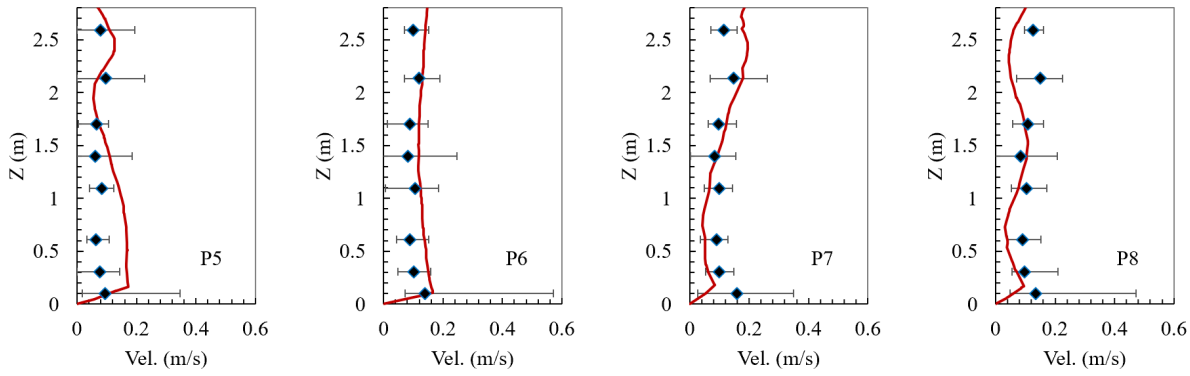

(b)

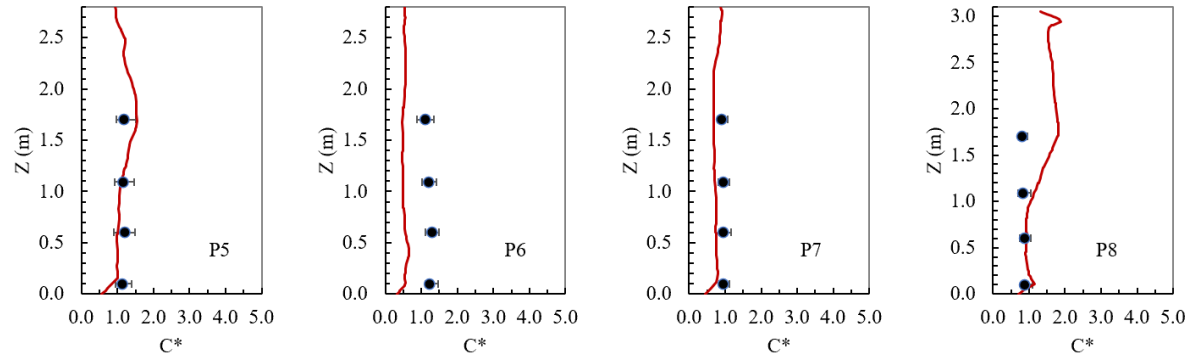

(c)

Fig. 8. Measured and simulated results in the room with the MV system under 4 ACH: (a) air temperature, (b) air velocity, and (c) normalized particle concentration, $C^*=(C-C_s)/(C_e-C_s)$, where C, C_e, and C_s are the contaminant concentration at a particular location, at the exhaust, and at the supply, respectively. Symbols: measurement; lines: simulation.

3.2 Air distribution in the room with the displacement ventilation system under 4 ACH

This section summarizes the flow characteristics of the DV system with 4 ACH. Fig. 9 presents the simulated velocity and temperature distributions in the center section of the room. Compared with the results computed for the MV system, the air velocity was lower and the air temperature had a stratification under the DV system. We used the random blocking method to simulate the velocity at the diffuser. The air velocity in front of the diffuser was not uniform, as shown in Fig. 9(a). Cool air was supplied to the lower level of the room with low momentum in the DV system. Therefore, the supplied air spread through the lower level of the room due to thermal buoyancy until it reached the heated manikins and computers in the center zone of the room. The air rose upward with the thermal plumes generated by the heated objects. The temperature gradient in the lower part of the room was much larger than that in the upper part of the room, as shown in Fig. 9(b).

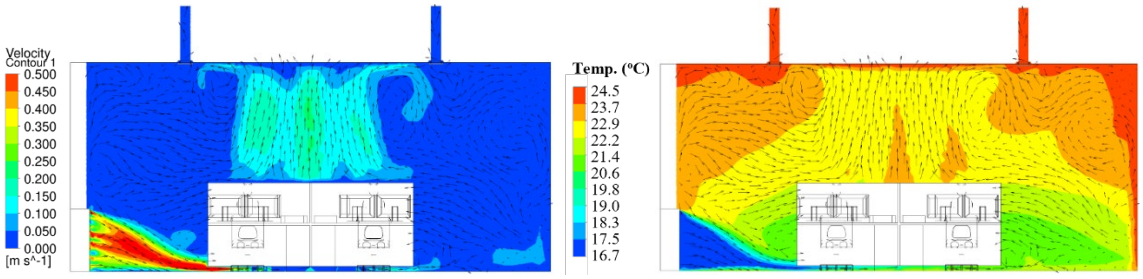

(a) (b)

Fig. 9. Simulated air velocity and temperature distributions in the center section of the room: (a) velocity distribution and (b) temperature distribution.

Fig. 10(a) and (b) present the simulated particle distribution in the section through the person who was the particle source. Fig. 10(c) and (d) show the corresponding velocity distribution at the same position as that for the particles. The particles were concentrated mainly in the upper part of the office. This is because the clean air was induced from the floor level and then traveled upward, bringing the particles into the upper zone. In addition, the particle concentration in the breathing zone of the other person was much lower than that under the MV system, as shown in Fig. 7. The high concentration in the bottom right corner was due to the vortex generated near the floor, as shown in Fig.10 (c). The particles were easily trapped in the recirculation zone. The partition board on the table also reduced the horizontal transmission of the particles. The DV system provided better indoor air quality than the MV system. The DV system can enhance the ventilation performance and reduce the risk of airborne infection indoors compared with the MV system.

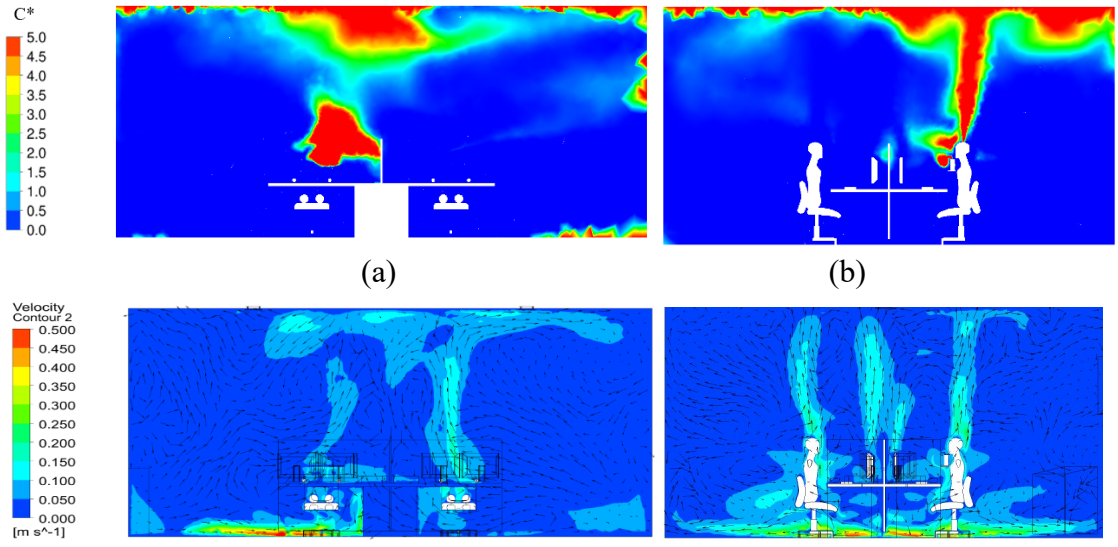

(a) (b)

(c) (d)

Fig. 10. Simulated particle concentration and air velocity distributions in the section through the particle-source individual in the room: (a) front view of the particle concentration distribution, (b) side view of the particle concentration distribution, (c) front view of the velocity distribution, and (d) side view of the velocity distribution.

Fig. 11 compares the measured and computed air temperature, air velocity, and particle concentration in the office with the DV system under 4 ACH. Locations P5, P6, P7, and P8 are shown in Fig. 3. With displacement ventilation, both the predicted and measured profiles exhibit a clear stratification.

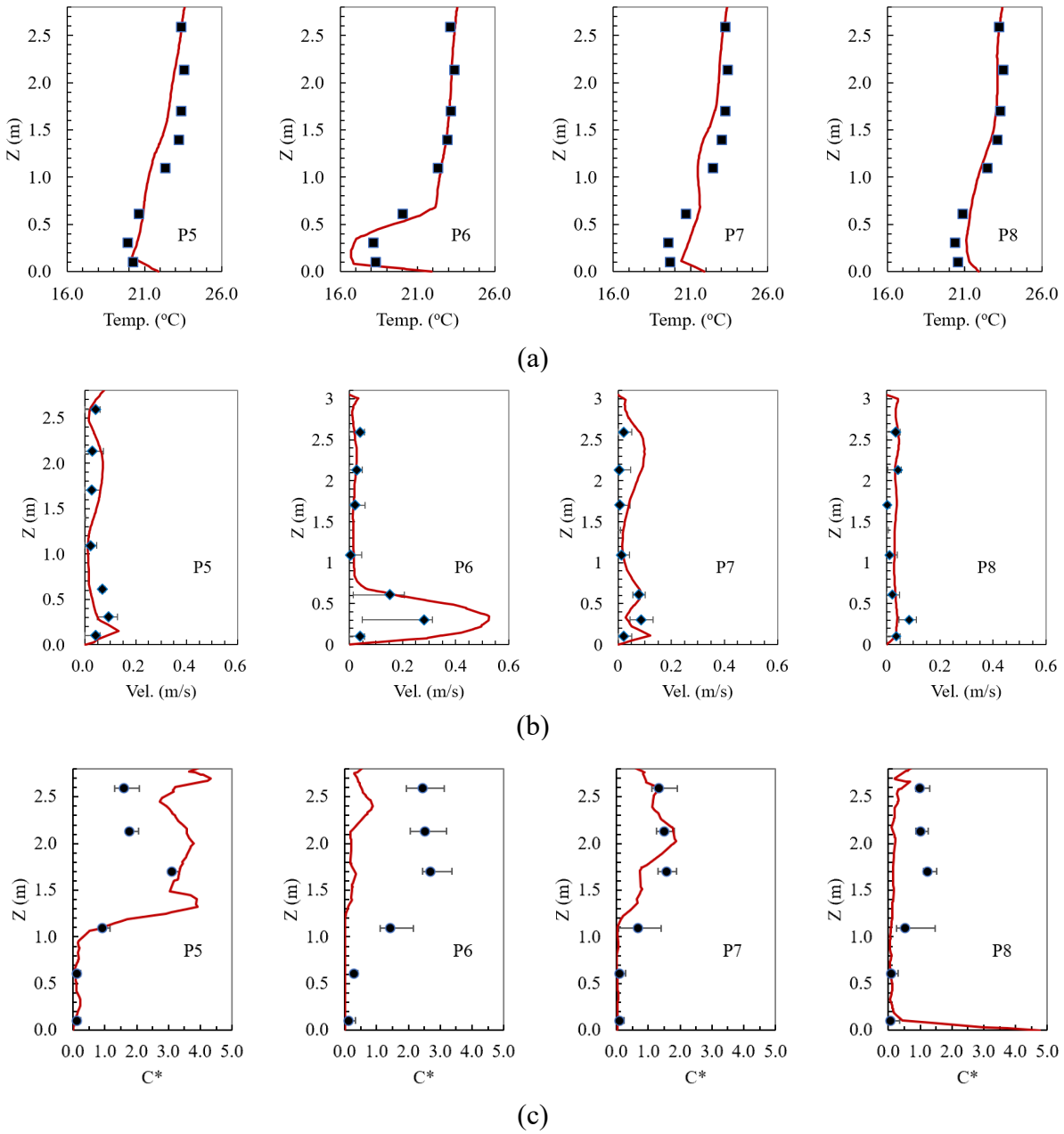

Fig. 11. Measured and simulated results in the room with the DV system under 4 ACH: (a) air temperature, (b) air velocity, and (c) normalized particle concentration, $C^*=(C-C_s)/(C_e-C_s)$, where C, C_e, and C_s are the contaminant concentration at a particular location, at the exhaust, and at the supply, respectively. Symbols: measurement; lines: computation.

Since P6 was located in front of the diffuser, the temperature in the lower part of P6 was much lower than that in other locations. In addition, the velocity in the lower part of P6 was larger than that in other locations. The air velocity in the room was lower than 0.05 m/s, except near the floor in P6 due to its proximity to the diffuser. The hot-sphere anemometers may have failed to accurately measure such a low velocity, so the measured data had high uncertainty. Since the particle concentration in the occupied zone was much lower than that in the upper zone, as shown in Fig. 11(c), the DV system provided better indoor air quality than the MV system.

The simulated results agreed reasonably well with the measured data. The maximum differences between the simulated results and the measured data for the air temperature, air

velocity, and normalized particle concentration were 1 ºC, 0.2 m/s, and 2.5, respectively. The simulated velocity at most measuring points was within the error range, except near the floor level at position P6. The simulation overestimated the air velocity. For particle concentration, the largest difference was also at P6. The simulated particle concentration was lower than the measured data. The simplification of the geometry, boundary conditions, etc., may have contributed to some uncertainties.

3.3 Comparison of the two ventilation systems with different ventilation rates

This section compares airflow characteristics between the two ventilation systems under different ventilation rates. Fig. 12 shows the temperature and velocity profiles at position P7. To maintain a similar indoor thermal environment, the air supply temperature was increased with the air change rate, as shown in Table 2 in Section 2.2. Therefore, the air temperature at different locations did not vary greatly with the airflow rate. The air velocity under the MV system increased with the ACH. Under the DV system, the air velocity did not exhibit a significant difference, except in the lower part of the room.

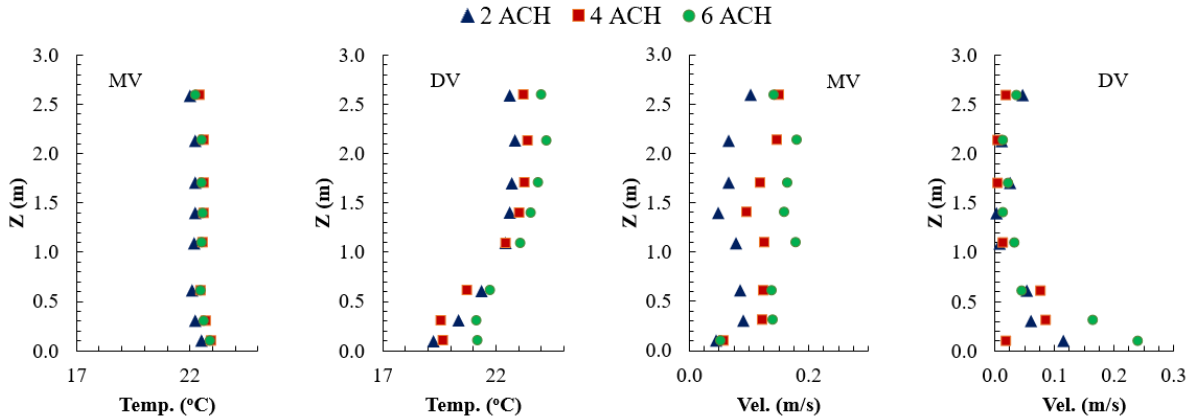

Fig. 12. Comparison of (a) air temperature profiles and (b) air velocity profiles for the MV and DV systems at position P7. (Blue triangles: 2 ACH; red squares: 4 ACH; green dots: 6 ACH.)

Fig. 13(a) shows the particle number concentration profiles under the MV system with different ventilation rates. The increase in ventilation rate from 2 ACH to 4 ACH reduced the particle concentration by 20%, and the increase from 2 ACH to 6 ACH reduced the concentration by 60%, on average. However, for the DV system, as depicted in Fig. 13(b), increasing the ventilation rate from 2 ACH to 4 ACH reduced the particle concentration by only 10%, and an increase from 2 ACH to 6 ACH caused a reduction of 40%. The DV system could not effectively remove the particles through an increase in ventilation rate, compared with the MV system. This is because the air velocity in the upper part of the room did not differ greatly under different ventilation rates with the DV system. An increase in ventilation rate can reduce the particle concentration under the two systems. However, the improvement was not proportional to the ventilation rate.

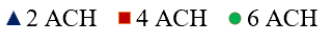

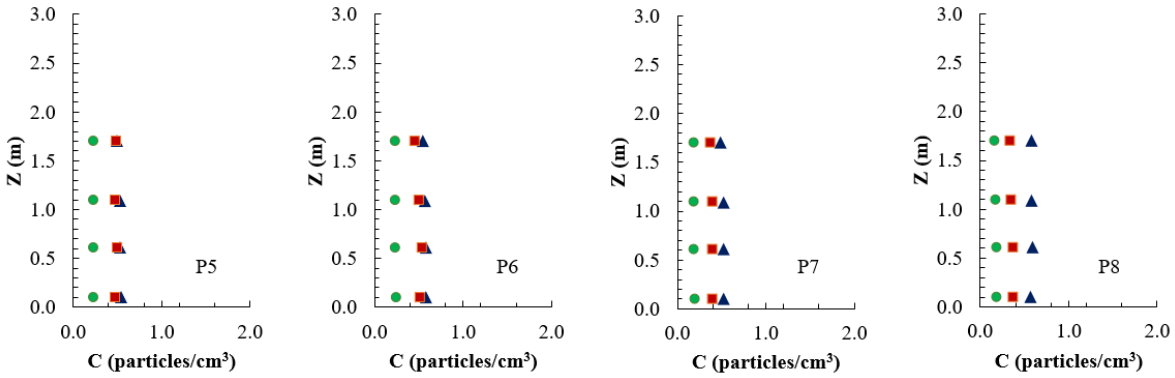

(a)

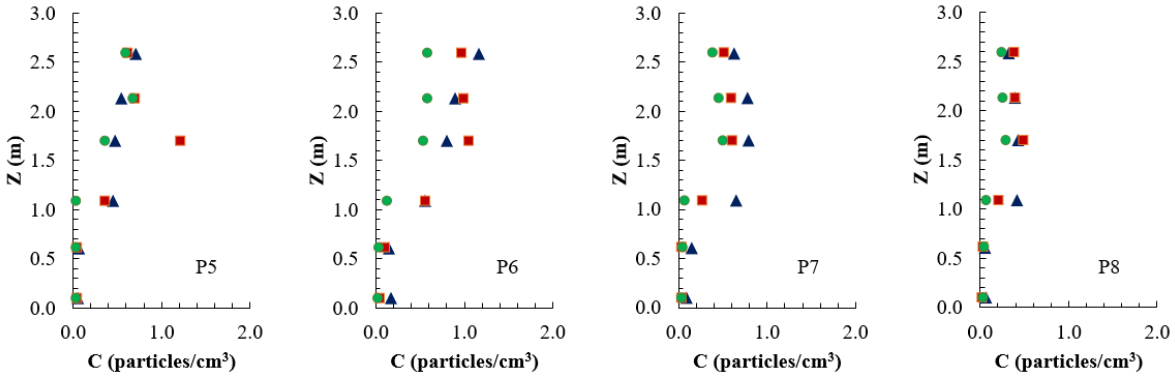

(b)

Fig. 13. Comparison of particle number concentration at different locations under different ventilation rates for (a) the MV system and (b) the DV system. (Blue triangles: 2 ACH; red squares: 4 ACH; green dots: 6 ACH.)

Table 4 summarizes the average ventilation effectiveness of the two ventilation systems with different ventilation rates. The average ventilation effectiveness ($VE_{a\text{-}1.1m}$) at the breathing zone is the average value of four measuring points at a height of 1.1 m above the floor. While the room average effectiveness ($VE_{a\text{-}room}$) is the average value at all measuring locations in the room. The MV system had average ventilation effectiveness of 0.97, 1.00, and 1.10, respectively, at the breathing zone under the three ventilation rates, while the values for the DV system were 1.07, 1.29, and 6.05, respectively. The MV system had the room average effectiveness of 0.97, 0.99, and 1.08, respectively, under the three ventilation rates, while the values for the DV system were 2.82, 3.79, and 5.52, respectively. The DV system was clearly superior to the MV system.

Table 4. Ventilation effectiveness of the two ventilation modes under different air change rates

	ACH	$VE_{a\text{-}1.1m}$	$VE_{a\text{-}room}$	C_e (particles/cm³)
MV	2	0.97	0.97	0.53
	4	1.00	0.99	0.42
	6	1.10	1.08	0.22
DV	2	1.07	2.82	0.53
	4	1.29	3.79	0.39
	6	6.05	5.52	0.38

4. Discussion

This investigation found that an increase in ventilation rate can reduce the particle concentration under the two systems. However, the improvements were not proportional to the ventilation rate. The increase in ventilation rates would have a significant impact on energy consumption [65]. To better control the airborne disease transmission, more measures should be syntheticly used [66], applying physical distancing [67], and adopting ultraviolet germicidal irradiation (UVGI) for air disinfection applications [68], etc.

In this paper, we modeled the particle transmission with a particle size of 0.4 μm that was generated for breathing. However, coughing, sneezing, and talking were with a high initial velocity and a wide range of particle size that may result in different transport behavior in the two ventilation modes. Previous investigations [19] found that particles larger than 10.0 μm may be too heavy to be carried upwards by the upward flow and remained at the human breathing height in DV, which may result in a higher level of pollution exposure than in MV. The performance of DV thus appears to be particle-size sensitive if the air velocity is too small. In addition, this investigation only simulated one particle source location, which was from the mouth of one index person. Tian et al. [21] found that exposure to contaminant was sensitive to the source locations under DV. While the source locations have little influence on the performance of MV. In addition, the particle deposition on walls and being breathed into the lung of the susceptible person was neglected in this investigation, which may lead to some errors.

This investigation had the following limitations:

- For the DV system, this study employed a user-defined function from Zhang et al. [51] to describe the face velocity on the diffuser. The opening distribution on the diffuser face was random. In addition, the shape and size of each cell were determined by the mesh distribution and size, and were different from the dimensions of the actual perforated openings. Therefore, some errors may have been introduced.
- The differences between the simulated results and the measured data for the DV system were larger than those for the MV system. The air velocity was low under the DV system, and the air pattern at this low velocity was not stable. Such a low-Reynolds-number flow was difficult to simulate by CFD with a high-Reynolds-number turbulence model. The simulations may have had high uncertainties. At the same time, measurements of the low air velocity with the hot-sphere anemometers may have produced very high errors. If the velocity cannot be accurately simulated and measured, the errors in measuring air temperature and particle number concentration will be large as well.
- This investigation assumed that there was no particle deposition, so particles were reflected once they reached a wall. This assumption may not be true, since some particles would have been trapped on the walls. Previous investigations [69,70,71] found that whether a particle would be trapped or reflected depends on the particle diameter, particle velocity, wall roughness, etc. Unfortunately, no information was available from the literature in regard to setting the ratio of rebounded and trapped particles. Errors were undoubtedly caused by our assumption, but we do not know their magnitude.
- Pan et al. [72] found that smaller particles with larger velocities were less likely to be deposited on superhydrophobic surfaces. Increasing the surface energy of the rough surface can significantly enhance the particle deposition rate owing to the strong particle–surface adhesion force. Further, appropriate surface roughness can reduce particle–surface adhesion and particle energy dissipation during collision, thereby leading to a deposition reduction. Lopes et al. [73] compared the performance of different particle-wall interaction models on the prediction of particle deposition on

walls. More accurate particle deposition on walls should be considered in future investigations.

- This investigation did not accurately simulate the process of particles being breathed into the lung of the susceptible person. Instead, we assumed if the particles were suspended in the breathing zone of the susceptible person, the particles may be breathed in by the person. However, the understanding of fine particle transport and deposition in the respiratory tract of the lung is important for the prediction of particle exposure [74].
- Particles with a diameter less than 1.0 μm have been found to exhibit different types of aerodynamic behavior when compared to particles with a diameter greater than 1.0 μm [70]. This investigation mainly focused on particles with a diameter of 0.4 μm, which corresponds to the diameter of particles generated through breathing. Additional particle diameters should be considered in future studies.

5. Conclusions

This investigation compared the airflow velocity, air temperature, and particle number concentration in an office under MV and DV systems with different ventilation rates. Both numerical simulations and experimental measurements were used. The study led to the following conclusions:

- The agreement between the computed results and measured data was reasonably good for engineering applications. The numerical simulations were much easier and cheaper than the experimental measurements. Therefore, the validated numerical model can be used as a tool for such applications.
- In the MV system, the air temperature was highly uniform at different locations along a vertical line. The air velocity in most positions in the room under 4 ACH was lower than 0.2 m/s. In the DV system, on the other hand, the air temperature and particle number concentration had a vertical gradient. The air velocity in the DV system was lower than that in the MV system.
- The DV system provided better indoor air quality than the MV system. This is because clean air was supplied in the lower part of the room under the DV system; thermal plumes from heated objects brought particles to the upper part of the room, and the exhaust was at ceiling level. This airflow pattern created a clean lower zone and a polluted upper zone with clear particle stratification. The particle number concentration in the breathing zone under the DV system was much lower than that under the MV system.
- This investigation found that the performance of the DV system depended on the contaminant source location and the associated heat source strength.
- An increase in ventilation rate can reduce the particle number concentration. However, the particle concentration reduction was not proportional to the change in ventilation rate. In the DV system, the decrease in the particle concentration with increasing ventilation rate was not very evident. However, the ventilation effectiveness increased significantly with the ventilation rate in the DV system, whereas the ventilation effectiveness remained close to 1.0 in the MV system. Hence, the DV system was clearly superior to the MV system.

Acknowledgments

This study was partially supported by the National Natural Science Foundation of China (NSFC) through grant No. 52108084, and by the China Postdoctoral Science Foundation through Grant No. 2020M680886.

References

[1] Iyanda A E, Adeleke R, Lu Y, et al. A retrospective cross-national examination of COVID-19 outbreak in 175 countries: a multiscale geographically weighted regression analysis. Journal of Infection and Public Health, 2020, 13(10): 1438-1445.
[2] https://coronavirus.jhu.edu/
[3] Van Doremalen N, Bushmaker T, Morris D H, et al. Aerosol and surface stability of SARS-CoV-2 as compared with SARS-CoV-1. New England Journal of Medicine, 2020, 382(16): 1564-1567.
[4] Fears A C, Klimstra W B, Duprex P, et al. Persistence of severe acute respiratory syndrome coronavirus 2 in aerosol suspensions. Emerging Infectious Diseases, 2020, 26(9): 2168.
[5] Lednicky J A, Lauzard M, Fan Z H, et al. Viable SARS-CoV-2 in the air of a hospital room with COVID-19 patients. International Journal of Infectious Diseases, 2020, 100: 476-482.
[6] Vuorinen V, Aarnio M, Alava M, et al. Modelling aerosol transport and virus exposure with numerical simulations in relation to SARS-CoV-2 transmission by inhalation indoors. Safety Science, 2020, 130: 104866.
[7] ASHRAE. Position document on infectious aerosols. American Society of Heating, Refrigerating and Air-Conditioning Engineers, 2020.
[8] Li Y, Leung G M, Tang J W, et al. Role of ventilation in airborne transmission of infectious agents in the built environment-a multidisciplinary systematic review. Indoor Air, 2007, 17(1): 2-18.
[9] Kaczmarczyk J, Melikov A, Fanger P O. Human response to personalized ventilation and mixing ventilation. Indoor Air, 2004, 14: 17-29.
[10] Behne M. Indoor air quality in rooms with cooled ceilings: Mixing ventilation or rather displacement ventilation?. Energy and Buildings, 1999, 30(2): 155-166.
[11] Yuan X, Chen Q, Glicksman L R. A critical review of displacement ventilation. ASHRAE Transactions, 1998, 104: 78.
[12] Kong X, Guo C, Lin Z, et al. Experimental study on the control effect of different ventilation systems on fine particles in a simulated hospital ward. Sustainable Cities and Society, 2021: 103102.
[13] Qian H, Li Y, Nielsen P V, et al. Dispersion of exhaled droplet nuclei in a two-bed hospital ward with three different ventilation systems. Indoor Air, 2006, 16(2): 111-128.
[14] Lin Z, Lee C K, Fong S, et al. Comparison of annual energy performances with different ventilation methods for cooling. Energy and Buildings, 2011, 43(1): 130-136.
[15] Ahmed A Q, Gao S, Kareem A K. A numerical study on the effects of exhaust locations on energy consumption and thermal environment in an office room served by displacement ventilation. Energy Conversion and Management, 2016, 117: 74-85.
[16] Hirnikel D J. Validation of a CFD model for temperature and particulate concentration in a test room with mixed air and displacement ventilation/Discussion. ASHRAE Transactions, 2003, 109: 80.
[17] Li X, Niu J, Gao N. Spatial distribution of human respiratory droplet residuals and exposure risk for the co-occupant under different ventilation methods. HVAC&R Research, 2011, 17(4): 432-445.
[18] Yin Y, Xu W, Gupta J K, et al. Experimental study on displacement and mixing ventilation systems for a patient ward. HVAC&R Research, 2009, 15(6): 1175-1191.
[19] Gao N, Niu J, Morawska L. Distribution of respiratory droplets in enclosed environments under different air distribution methods. Building Simulation, 2008, 1(4): 326-335.
[20] Buus M, Winther FV, Thilageswaran M. Contaminant flow in the microenvironment between people under different ventilation conditions. ASHRAE Transactions, 2008, 114: 632.
[21] Tian X, Li B, Ma Y, et al. Experimental study of local thermal comfort and ventilation performance for mixing, displacement and stratum ventilation in an office. Sustainable Cities and Society, 2019, 50: 101630.

[22] Dai H, Zhao B. Association of the infection probability of COVID-19 with ventilation rates in confined spaces. Building Simulation, 2020, 13(6): 1321-1327.
[23] Myatt T A, Johnston S L, Zuo Z, et al. Detection of airborne rhinovirus and its relation to outdoor air supply in office environments. American Journal of Respiratory and Critical Care Medicine, 2004, 169(11): 1187-1190.
[24] Kulkarni H, Smith C M, Lee D D H, et al. Evidence of respiratory syncytial virus spread by aerosol. Time to revisit infection control strategies? American Journal of Respiratory and Critical Care Medicine, 2016, 194(3): 308-316.
[25] Sornboot J, Aekplakorn W, Ramasoota P, et al. Detection of airborne Mycobacterium tuberculosis complex in high-risk areas of health care facilities in Thailand. The International Journal of Tuberculosis and Lung Disease, 2019, 23(4): 465-473.
[26] ASHRAE. Epidemic Task Force Resources on Building Guides: Commercial. American Society of Heating, Refrigerating and Air-Conditioning Engineers, 2020.
[27] REHVA, COVID R. Guidance document: how to operate and use building services in order to prevent the spread of the coronavirus disease (COVID-19) virus (SARSCoV-2) in workplaces, the Federation of European Heating, Ventilation and Air-Conditioning Associations, 2020: 19.
[28] CDC. Interim Guidance for Businesses and Employers Responding to Coronavirus Disease 2019 (COVID-19), Centers for Disease Control and Prevention, 2020.
[29] WHO. Considerations for quarantine of contacts of COVID-19 cases: interim guidance, World Health Organization, 2020.
[30] Walker J T, Hoffman P, Bennett A M, et al. Hospital and community acquired infection and the built environment–design and testing of infection control rooms. Journal of Hospital Infection, 2007, 65: 43-49.
[31] Memarzadeh F, Xu W. Role of air changes per hour (ACH) in possible transmission of airborne infections. Building Simulation, 2012, 5(1): 15-28.
[32] Mousavi E S, Grosskopf K R. Ventilation rates and airflow pathways in patient rooms: A case study of bioaerosol containment and removal. Annals of Occupational Hygiene, 2015, 59(9): 1190-1199.
[33] Li X, Zhang T T, Fan M, et al. Experimental evaluation of particle exposure at different seats in a single-aisle aircraft cabin. Building and Environment, 2021: 108049.
[34] Lee K, Zhang T, Jiang Z, et al. Comparison of airflow and contaminant distributions in rooms with traditional displacement ventilation and under-floor air distribution systems. ASHRAE Transactions, 2009, 115(2): 306-321.
[35] Shi Z, Chen J, You R, et al. Modeling of gasper-induced jet flow and its impact on cabin air quality. Energy and Buildings, 2016, 127: 700-713.
[36] Liu S, Zhao X, Nichols S R, et al. Evaluation of airborne particle exposure for riding elevators. Building and Environment, 2022, 207: 108543.
[37] Coleman H W, Stern F. Uncertainties and CFD code validation. 1997, 795-803.
[38] Sia S F, Yan L M, Chin A W H, et al. Pathogenesis and transmission of SARS-CoV-2 in golden hamsters. Nature, 2020, 583(7818): 834-838.
[39] Richard M, Kok A, de Meulder D, et al. SARS-CoV-2 is transmitted via contact and via the air between ferrets. Nature Communications, 2020, 11(1): 1-6.
[40] Hadei M, Hopke P K, Jonidi A, et al. A letter about the airborne transmission of SARS-CoV-2 based on the current evidence. Aerosol and Air Quality Research, 2020, 20(5): 911-914.
[41] Asadi S, Bouvier N, Wexler A S, et al. The coronavirus pandemic and aerosols: Does COVID-19 transmit via expiratory particles?. Aerosol Science and Technology, 2020, 54(6): 635-638.
[42] Gupta J K, Lin C H, Chen Q. Transport of expiratory droplets in an aircraft cabin. Indoor Air, 2011, 21(1): 3-11.
[43] Morawska L. Droplet fate in indoor environments, or can we prevent the spread of infection? Indoor Air. 2006, 16(5):335-47.
[44] Subbarao K, Mahanty S. Respiratory virus infections: understanding COVID-19. Immunity, 2020, 52(6): 905-909.
[45] ISO I. Energy performance of buildings-Indoor environmental quality-Part 1: Indoor environmental input parameters for the design and assessment of energy performance of buildings. 2017.

[46] UNI E N. Energy Performance of Buildings-Ventilation for Buildings-Part 1: Indoor Environmental Input Parameters for Design and Assessment of Energy Performance of Buildings Addressing Indoor Air Quality. Thermal Environment, Lighting and Acoustics, 2019: 16798-1.
[47] WHO. Roadmap to improve and ensure good indoor ventilation in the context of COVID-19. World Health Organization, 2021.
[48] ANSYS Inc.. ANSYS Fluent 14.0 User's Guide. ANSYS Inc. Southpointe. 2011.
[49] Shih T H, Liou W W, Shabbir A, et al. A new k-ε eddy viscosity model for high Reynolds number turbulent flows. Computers & Fluids, 1995, 24(3): 227-238.
[50] Gray D D, Giorgini A. The validity of the Boussinesq approximation for liquids and gases. International Journal of Heat and Mass Transfer, 1976, 19(5): 545-551.
[51] Zhang T, Lee K, Chen Q. A simplified approach to describe complex diffusers in displacement ventilation for CFD simulations. Indoor Air, 2009, 19(3): 255-267.
[52] Zhao B, Zhang Y, Li X, et al. Comparison of indoor aerosol particle concentration and deposition in different ventilated rooms by numerical method. Building and Environment, 2004, 39(1): 1-8.
[53] Li A, Ahmadi G. Dispersion and deposition of spherical particles from point sources in a turbulent channel flow. Aerosol Science and Technology, 1992, 16(4): 209-226.
[54] Zhang H, Wang F, Wang Y, et al. CFD Simulation of cooking particle distribution and motion. Procedia Engineering, 2017, 205: 1800-1806.
[55] Elghobashi S. On predicting particle-laden turbulent flows. Applied Scientific Research, 1994, 52(4): 309-329.
[56] Chen C, Liu W, Lin C H, et al. Comparing the Markov chain model with the Eulerian and Lagrangian models for indoor transient particle transport simulations. Aerosol Science and Technology, 2015, 49(10): 857-871.
[57] Chen C, Liu W, Lin C H, et al. Accelerating the Lagrangian method for modeling transient particle transport in indoor environments. Aerosol Science and Technology, 2015, 49(5): 351-361.
[58] Chen C, Lin C-H, Wei D, et al. Modeling particle deposition on the surfaces around a multi-slot diffuser. Building and Environment, 2016, 107:79-89.
[59] Zhang Z, Chen, Q. Experimental measurements and numerical simulations of particle transport and distribution in ventilated rooms. Atmospheric Environment, 2006, 40(18): 3396-3408.
[60] GAMBIT CFD Preprocessor. User's Guide. Lebanon, NH: Fluent Inc. 1998.
[61] Fleming K K, Longmire E K, Hubel A. Numerical characterization of diffusion-based extraction in cell-laden flow through a microfluidic channel. Journal of Biomechanical Engineering, 2007, 129(5): 703-711.
[62] ASHRAE. Standard 62.1-2019 Ventilation for Acceptable Indoor Air Quality. American Society of Heating, Refrigerating and Air-Conditioning Engineers, Inc., Atlanta, GA, 40.
[63] Shi Z, Chen Q. Experimental and computational investigation of wall-mounted displacement induction ventilation system. Energy and Buildings, 2021, 241: 110937.
[64] Rim D, Novoselac A. Ventilation effectiveness as an indicator of occupant exposure to particles from indoor sources. Building and Environment, 2010, 45(5): 1214-1224.
[65] Fisk W J, Black D, Brunner G. Changing ventilation rates in US offices: Implications for health, work performance, energy, and associated economics. Building and Environment, 2012, 47: 368-372.
[66] Powell V D, Silveira M J. What should palliative care's response be to the COVID-19 pandemic?. Journal of Pain and Symptom Management, 2020, 60(1): 1-3.
[67] Sun C, Zhai Z. The efficacy of social distance and ventilation effectiveness in preventing COVID-19 transmission. Sustainable Cities and Society, 2020, 62: 102390.
[68] Hamzavi I H, Lyons A B, Kohli I, et al. Ultraviolet germicidal irradiation: Possible method for respirator disinfection to facilitate reuse during the COVID-19 pandemic. Journal of the American Academy of Dermatology, 2020, 82(6): 1511-1512.
[69] Thatcher T L, Lai A C K, Moreno-Jackson R, et al. Effects of room furnishings and air speed on particle deposition rates indoors. Atmospheric Environment, 2002, 36(11): 1811-1819.
[70] Lai A C K. Particle deposition indoors: A review. Indoor Air, 2002, 12(4): 211-214.
[71] Mukai C, Siegel J A, Novoselac A. Impact of airflow characteristics on particle resuspension from indoor surfaces. Aerosol Science and Technology, 2009, 43(10): 1022-1032.

[72] Pan A, Cai R R, Zhang L Z. Numerical methodology for simulating particle deposition on superhydrophobic surfaces with randomly distributed rough structures. Applied Surface Science, 2021, 568: 150872.
[73] Lopes M B, Mariani V C, Mendonça K C, et al. On the use of particle-wall interaction models to predict particle-laden flow in 90-deg bends. Building Simulation, 2020, 13(4): 913-929.
[74] Sommerfeld M, Sgrott Jr O L, Taborda M A, et al. Analysis of flow field and turbulence predictions in a lung model applying RANS and implications for particle deposition. European Journal of Pharmaceutical Sciences, 2021, 166: 105959.

Appendix I: Grid independence analysis

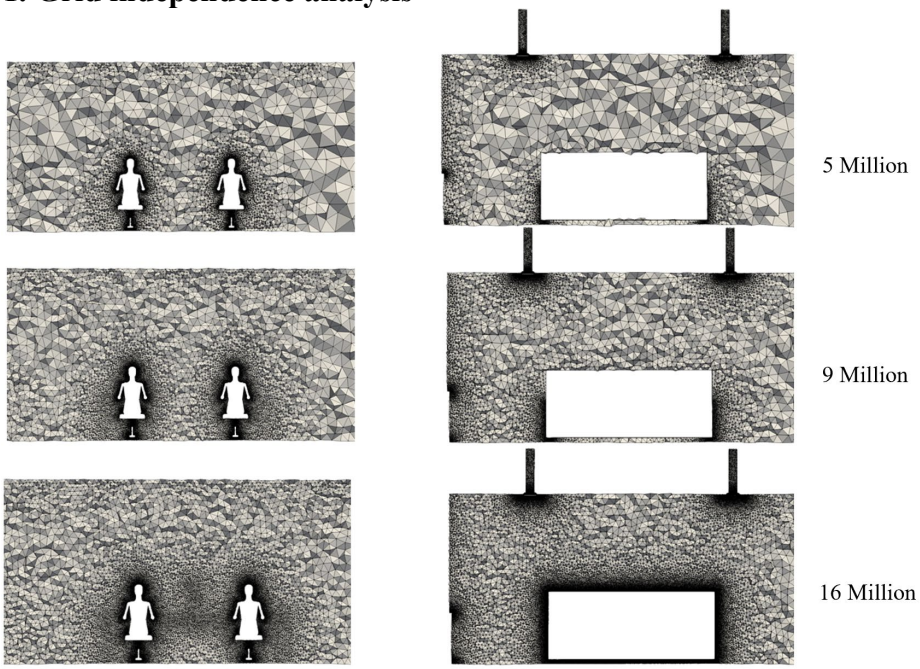

Fig.A1. Meshes for different grids number

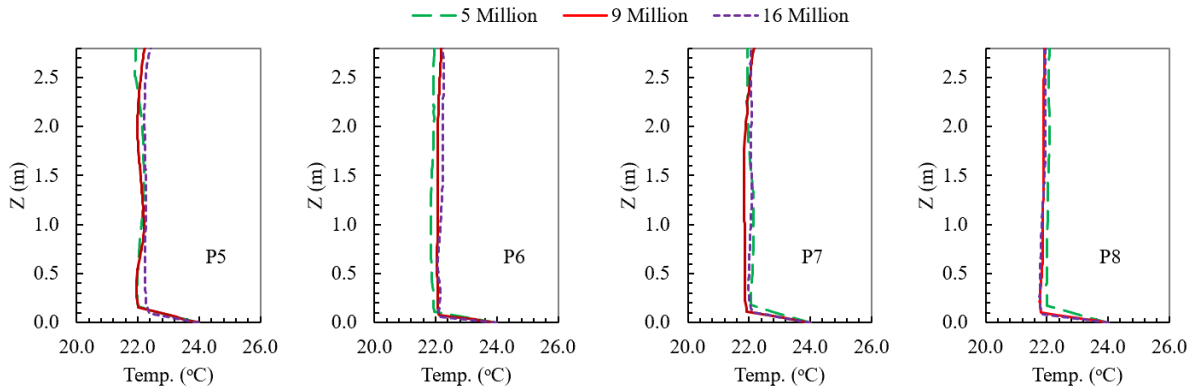

(a)

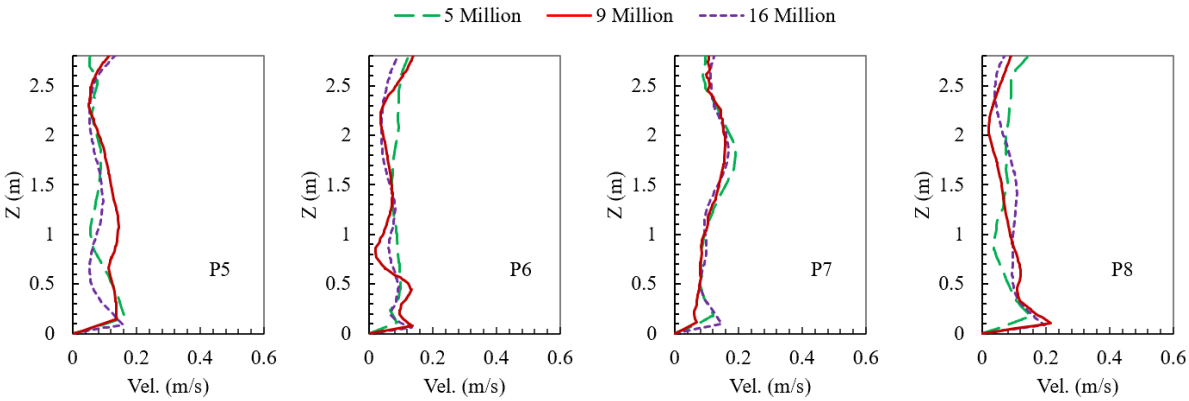

(b)

Fig.A2. Simulated results by different grids for: (a) air temperature, and (b) air velocity